ACS OMEGA

http://pubs.acs.org/journal/acsodf

Article

Histological Injury to Rat Brain, Liver, and Kidneys by Gold Nanoparticles is Dose-Dependent

Bekhti Sari Fadia, Nassima Mokhtari-Soulimane, Bensalah Meriem, Nacer Wacila, Badi Zouleykha, Rouigueb Karima, Tewfik Soulimane, Syed A. M. Tofail, Helen Townley, and Nanasaheb D. Thorat*

Cite This: *ACS Omega* 2022, 7, 20656−20665

Read Online

ACCESS | Metrics & More | Article Recommendations

ABSTRACT: Gold nanoparticles (GNPs) possess various interesting plasmonic properties that can provide a variety of diagnostic and therapeutic functionalities for biomedical applications. Compared to other inorganic metal nanoparticles (NPs), GNPs are less toxic and more biocompatible. However, the *in vivo* toxicity of gold nanoparticles on humans can be significant due to the size effect. This work aims to study the effect of multiple doses of small-size (≈20 nm) GNPs on the vital organs of Wistar rats. The study includes the oxidative stress in vital organs (liver, brain, and kidney) caused by GNPs and histopathology analysis. The rats were given a single caudal injection of NPs dispersed in PBS at 25, 50, 100, and 250 mg/kg of body weight. After sacrifice, both plasma and organs were collected for the determination of oxidant/antioxidant markers and histological studies. Our data show the high sensitivity of oxidative stress parameters to the GNPs in the brain, liver, and kidneys. However, the response to this stress is different between the organs and depends upon the antioxidant defense, where GSH levels control the MDA and PCO levels. Histological alterations are mild at 25, 50, and 100 mg/kg but significant at higher concentrations of 250 mg/kg. Therefore, histological impairments are shown to be dependent on the dose of GNPs. The results contribute to the understanding of oxidative stress and cellular interaction induced by nanoparticles.

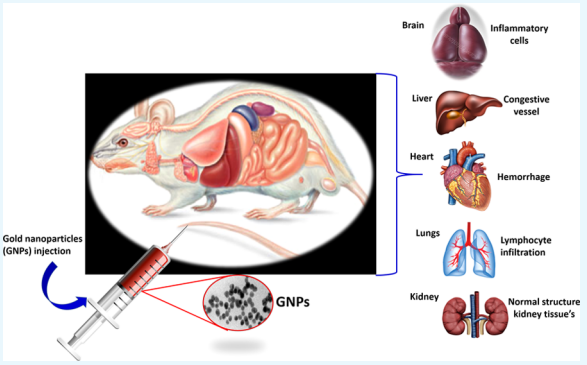

1. INTRODUCTION

Nanoparticles are materials ranging from 1 to 100 nm in one or more dimensions.[1] Gold nanoparticles (GNPs) are the most studied nanoscale material for medical applications, both as therapeutic and diagnostic tools. GNPs exhibit excellent colloidal stability along with the size-dependent surface plasmon resonance (SPR) and fluorescence properties and stable surface for further bioconjugation, allowing the use of GNPs in imaging diagnosis,[2] drug delivery,[3] radiosensitization,[4,5] photothermal therapy,[6,6a] radiotherapy,[7] cancer therapeutics, and gene therapy.[8] These small particles are rapidly taken into the system and partly accumulate in the targeted tissues. The small size and the large surface-area-to-volume ratio of nanoparticles (NPs) favor the conjugation of biomolecules more than their bulk counterparts.[8,9] As such, they are similar in scale to biological macromolecules. Some studies have reported that GNPs are not toxic while others have indicated toxic effects related to their functional surface attachment, charge, shape, and size.[10−12]

Previous studies have investigated the impact of the size of GNPs on tissue appearance[13,14] and effects related to the duration of exposure[15] and repeated administration.[16] These works have shown that smaller NPs induce higher cytotoxicity and immunological responses and that cell damage is increased with longer exposure times. In addition, repeated dosing with GNPs causes liver alterations. Other studies have examined the impact of the delivery route of GNPs on tissues, including inhalation,[17] intravenous,[18] and peritoneal administrations.[19] After the inhalation deposition, small gold nanoparticles are seen in the liver, spleen, brain, and testes. Intravenous injection of 13 nm GNPs induces acute inflammation and apoptosis in the mouse liver. Peritoneal injection of GNPs of different sizes causes structural changes in the kidneys and spleen of the mice. The GNPs with the smallest diameter (5 nm) produce significant pathological changes in the liver.[17−19]

It is also known that GNPs induce oxidative stress, e.g., reactive oxygen species (ROS), which is at the origin of tissue changes.[20,21] However, the mechanisms of oxidative stress and their regulation in response to nanoparticles are not well

Received: February 4, 2022
Accepted: May 24, 2022
Published: June 7, 2022

https://doi.org/10.1021/acsomega.2c00727
ACS Omega 2022, 7, 20656−20665

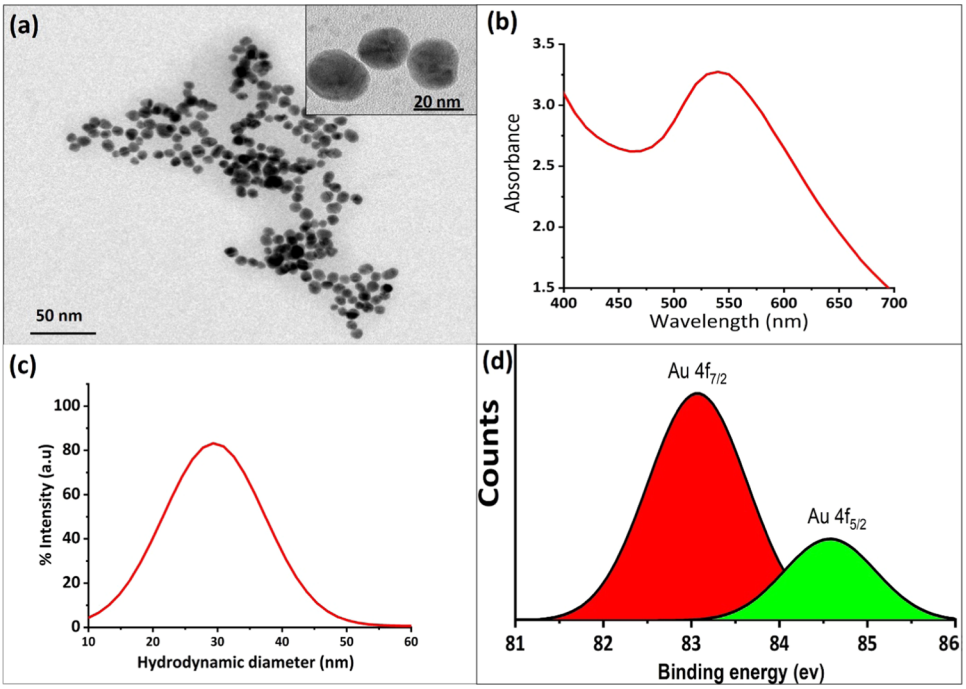

Figure 1. (a) TEM and (b) UV−vis spectroscopy results of GNPs. (c) Dynamic light spectra (DLS) of the GNPs. DLS results show that GNPs were less aggregated in water and homogeneously distributed with a size range of 20−40 nm. (d) X-ray photoelectron spectroscopy (XPS) studies of GNPs to confirm the structural analysis of the GNP formation.

known. This research aims to study the oxidative stress and histopathological changes induced by small diameter (≈20 nm) GNPs on the brain, liver, and kidney tissues of Wistar rats at 25, 50, 100, and 250 mg/kg concentrations. The histopathological study demonstrated which GNP doses resulted in oxidative stress-induced alterations at the cellular level. In addition, the safety of the chemically synthesized GNPs ≈20 nm is investigated after intravenous administration in a small animal model. Knowledge of the impact of doses of GNPs on tissues allows the safe use of these GNPs in biomedical applications, including cancer therapy and diagnosis.

2. EXPERIMENTAL SECTION

2.1. Gold Nanoparticle Synthesis. The 20 nm gold nanoparticles were synthesized using the "Inversed Turkevich" method.[22,23] Sodium citrate (1.0% w/v) solution was prepared in 20.0 mL of deionized water. The solution was heated to 95 °C for 15 min and then 1 mL of the $HAuCl_4$ stock solution (10 mM) was added to the boiling sodium citrate solutions under stirring. Within a minute, the solution color changed from yellow to dark pink, ensuring the formation of homogeneous GNPs. Furthermore, the solution was kept on a hot plate for 30 min to ensure the synthesis of homogeneous GNPs. The GNPs were collected via centrifugation (4000 rpm for 10 min) and stored at room temperature. For *in vivo* experiments, the nanoparticles were sterilized in an autoclave.

2.2. *In Vivo* Experiments. A total of 15 male Wistar rats obtained from the Pasteur Institute of Algiers, weighing 190 ± 10 g, were housed in spacious stainless steel cages. The raising of animals and all aspects of the experiments were conducted according to the policies of the University of Tlemcen Institutional Animal Care and Use Committee (IACUC) (Accreditation number: D01N01UN130120150006/2016). The rats were maintained under laboratory standard conditions (12/12 h light/dark cycle), temperature (20 ± 2 °C), and relative humidity (50 ± 15%). The animals had free access to food (standard diet) and water *ad libitum*. The study was conducted following the national guidelines for the care and use of laboratory animals. All of the experimental protocols were approved by the Regional Ethical Committee. The rats were divided into five groups (three rats per group) and subjected to a period of 15 days of adaptation. They received different doses of nanoparticles dissolved in PBS (25, 50, 100, and 250 mg/kg of body weight) by unique caudal injection, a direct and rapid vascular access route to all organs. The control group received a caudal injection containing PBS.

2.3. Sample Collection. Fifteen days after the caudal injection, the rats were fasted overnight and sacrificed. They were anesthetized with i.p. chloral 10% (w/v) (3 mL/kg bw). Blood was drawn from the abdominal aorta and centrifuged at 3000*g* for 15 min and the plasma was used for biochemical analyses and oxidative stress determination. Brain, liver, and kidneys were collected and thoroughly washed with an ice-cold 0.1 M phosphate buffer saline (PBS; pH 7.4). An aliquot of each tissue was homogenized in an Ultraturrax homogenizer (Bioblock Scientific, Illkirch, France) and homogenized in 10 volumes of an ice-cold 10 mM phosphate-buffered saline. The homogenate was subjected to 6000*g* centrifugation at 4 °C for 15 min. The supernatant fractions were collected and used for redox marker determinations. Histological samples were carefully removed with a sharp razor blade and fixed into 10% formol.[24]

2.4. Biochemical Parameters. Plasma albumin, creatinine, urea, and uric acid were measured using enzymatic test kits (Sigma Chemical Co., St. Louis, MO).

2.5. Oxidative Stress Markers. Glutathione (GSH) was measured in plasma and tissues using the method based on the reduction of 5,5′-dithiobis(2-nitrobenzoic acid) (DTNB) with reduced glutathione to produce a yellow compound. The

https://doi.org/10.1021/acsomega.2c00727
ACS Omega 2022, 7, 20656−20665

Table 1. Effects of Different Doses of Gold Nanoparticles on Albumin, Urea, Creatinine, and Uric Acid Levels[a]

	control	25 mg/kg	50 mg/kg	100 mg/kg	250 mg/kg
albumin (μM)	537.2 ± 5.4	53.4 ± 20.7	598.5 ± 18.9	546.2 ± 42.7	538.3 ± 64.4
urea (mg/dL)	20.7 ± 3.2	80.2 ± 4.1***	81.9 ± 5.6***	69.8 ± 1.8***	84.6 ± 5.9***
creatinine (mg/dL)	1.5 ± 0.5	1.9 ± 0.6	1.7 ± 0.4	4.9 ± 0.6***	6 ± 0.3***
uric acid (mg/dL)	6.9 ± 0.7	5.2 ± 1.7	5.5 ± 0.4	10.5 ± 0.3***	8.5 ± 0.8**

[a]Values are presented as mean ± SD. **P < 0.01 and ***P < 0.001.

reduced chromogen is directly proportional to the GSH concentration and its absorbance was measured at 405 nm.[25] Malondialdehyde (MDA) is a marker of lipid peroxidation, and the levels were measured in plasma and tissues by the reaction of MDA with thiobarbituric acid.[26] Protein carbonyls (PCOs) were assessed by the determination of the carbonyl group content based on the reaction with dinitrophenylhidrazine (DNPH), as previously described.[27] Proteins were precipitated by the addition of 20% trichloroacetic acid and redissolved in DNPH. The absorbance was monitored spectrophotometrically at 370 nm.

2.6. Histopathological Studies. Tissues collected from the animals were excised and dehydrated using grades of alcohol. Dehydration was followed by clearing the samples in two changes of xylene. The tissue samples are then impregnated with two changes of molten paraffin wax, immersed, and blocked out. Finally, tissues were sectioned by microtomy and attached to the surface of a glass slide for further staining and microscopic examination. Paraffin sections of 3 μm thickness were stained with hematoxylin and eosin (HE) and mounted on a glass slide of a microscope.[28] The HE stained tissue sections were observed and photographed using an optical microscope (AX80, Olympus, Tokyo, Japan). From the microscopic observations, alterations in tissue architecture, the presence of degeneration, necrosis, inflammation, and portal fibrosis tissue structures were observed.

2.7. Statistical Analysis. The analyzed parameters were statistically evaluated using Statistica (version 4.1; Statsoft, Paris, France). The results were expressed as mean ± standard deviation (SD). Comparisons between GNP-treated rats and control rats were performed using Student's t-test. Differences were considered statistically significant at *P < 0.05, **P < 0.01, and ***P < 0.001.

3. RESULTS AND DISCUSSION

3.1. Gold Nanoparticle Synthesis. Transmission electron microscopy (TEM) was used to determine the size, size distribution, and shape of GNPs. The particles were shown to be spherical with an average size of 20 ± 3 nm and narrow size distribution. The UV−vis spectrum of the GNPs indicated a single visible peak that was positioned in the range 519−531 nm and was related to the spherical monodispersed 20 nm GNPs (Figure 1a,b). The dynamic light spectra (DLS) showed that the GNPs were less aggregated in water and homogeneously distributed with a size range of 20−40 nm (Figure 1c). The size distribution of GNPs was calculated by generating a histogram of diameters of 100 NPs from the TEM image using ImageJ software. The polydispersity index (PDI) <0.10 was observed in DLS studies. The value of PDI <0.10 was an indication of homogeneous NPs. X-ray photoelectron spectroscopy (XPS) of the GNPs in Figure 1d shows a pair of signals at 83.6 and 84.5 eV. This reveals that the gold atoms exist in the Au^0 and Au^{3+} oxidation states in the GNPs.[29]

3.2. Mortality and Clinical Observation. No mortality or abnormal clinical signs or behavioral changes, such as skin and fur conditions, eye changes, diarrhea, abdominal breathing, and food consumption were observed in rats throughout the experimental period of GNPs treatment. No significant differences in mean body weight, weight gain, and relative weight were found compared to the control group (data not shown).

3.3. Biochemical Findings. Renal impairment was indicated by an increase in creatinine at higher GNP doses (100 and 250 mg/kg) in rats. Histological renal damage in 100 and 250 mg/kg GNPs treated rats was marked by several congestive vessels, tubular degeneration, and necrotic state. Urea was increased in all rats treated with GNPs, and uric acid showed a higher plasma level at 100 and 250 mg/kg GNPs. Large amounts of uric acid can be produced from tissue injury *in vivo* and promoted immune responses.[30] Microscopic observations demonstrated focal necrotic areas in the brain, liver, and kidneys at 250 mg/kg GNPs. The hyperuricemic rats developed renal disease with inflammatory cell infiltration and COX-2 expression (Table 1).[31,32]

3.4. Oxidative Stress and Histopathological Findings. NPs can cross biological barricades to reach internal organs, and this is size- and surface-dependent phenomenon. Earlier *in vivo* study report confirms the accumulation of metal NPs in all of the vital organs.[33] It is a well-established phenomenon that the size of NPs decreases with the increase in their surface-area-to-volume ratio. The higher the ratio is, the higher the number of atoms or molecules that are on the surface of NPs, resulting in increased surface reactivity.[34] The increased surface reactivity of NPs is responsible for the higher toxicity compared to their bulk counterpart.[35] NPs smaller than 20 nm have also been shown to be more injurious since they are able to pass through the nuclear membrane and cause DNA damage.[36] The current study reveals higher ROS production and proapoptotic induction by GNPs in the vital organ tissues. The shape of GNPs also affects the apoptosis level. It was demonstrated a strong proapoptotic marker including Fas, caspase 3 and caspase 9 expression in cells following exposure to hexagonal GNPs compared to spherical GNPs.[37] Hence, the interest in studying the effects of spherical GNPs on different organs is interesting for developing safe and biocompatible nanomaterials for biomedical applications.

Oxidative stress was observed in the systemic circulation 15 days after GNP caudal injection, displayed as an increase in lipid peroxidation (MDA) associated with the reduced GSH level in all rats treated with GNPs compared to controls. GSH, a sulfhydryl peptide widely found in all biological systems, forms the first line of defense against oxidative damage by acting as a nonenzymatic antioxidant.[38] GSH acts as a nucleophilic agent or as an antioxidant against electrophilic or oxidative compounds, resulting from endogenous or exogenous sources.[39] It is also a chelator of transition metals including gold.[40] Although the liver is a net synthesizer of

https://doi.org/10.1021/acsomega.2c00727
ACS Omega 2022, 7, 20656−20665

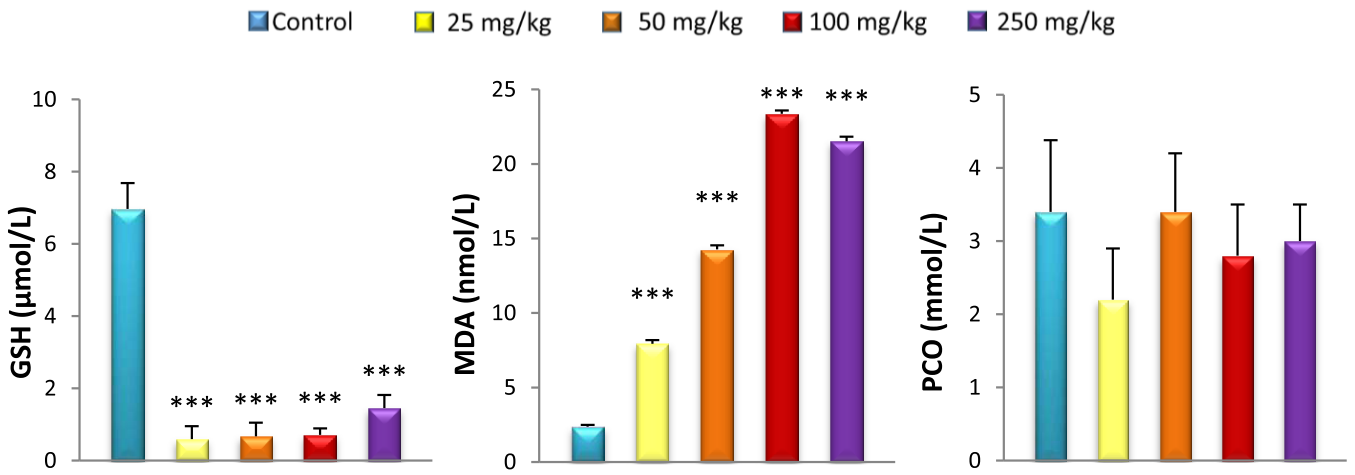

Figure 2. Effect of caudal injection of different doses of GNPs on plasma GSH, MDA, and PCO levels compared to control. Values were presented as mean ± SD. ***$P < 0.001$.

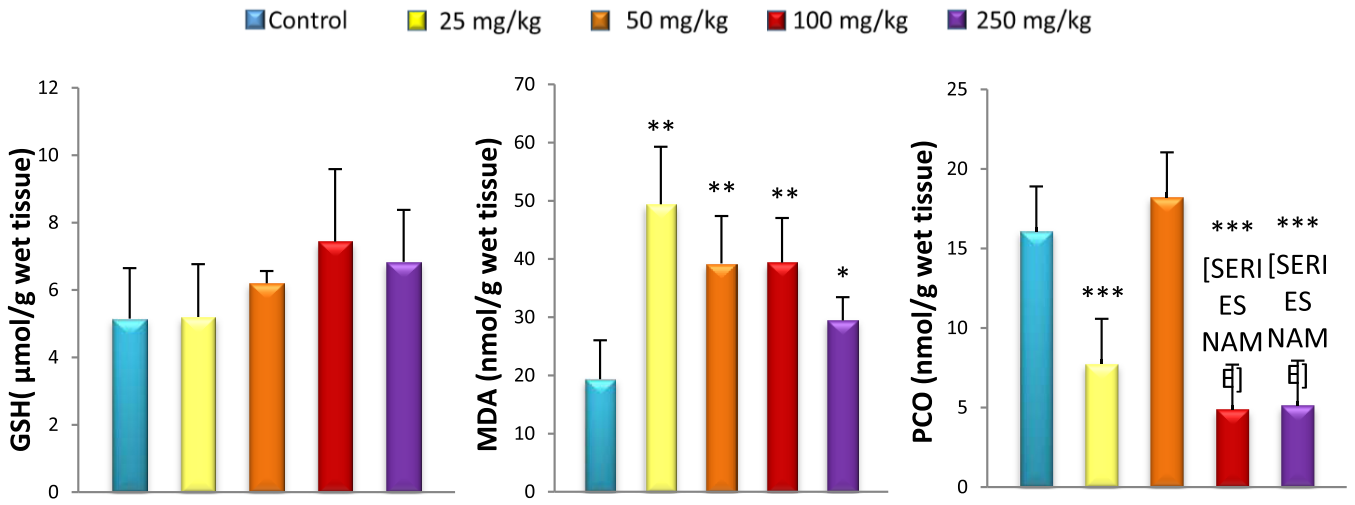

Figure 3. Effect of caudal injection of different doses of GNPs on liver GSH, MDA, and PCO levels compared to control. Values were presented as mean ± SD. *$P < 0.05$; **$P < 0.01$; ***$P < 0.001$.

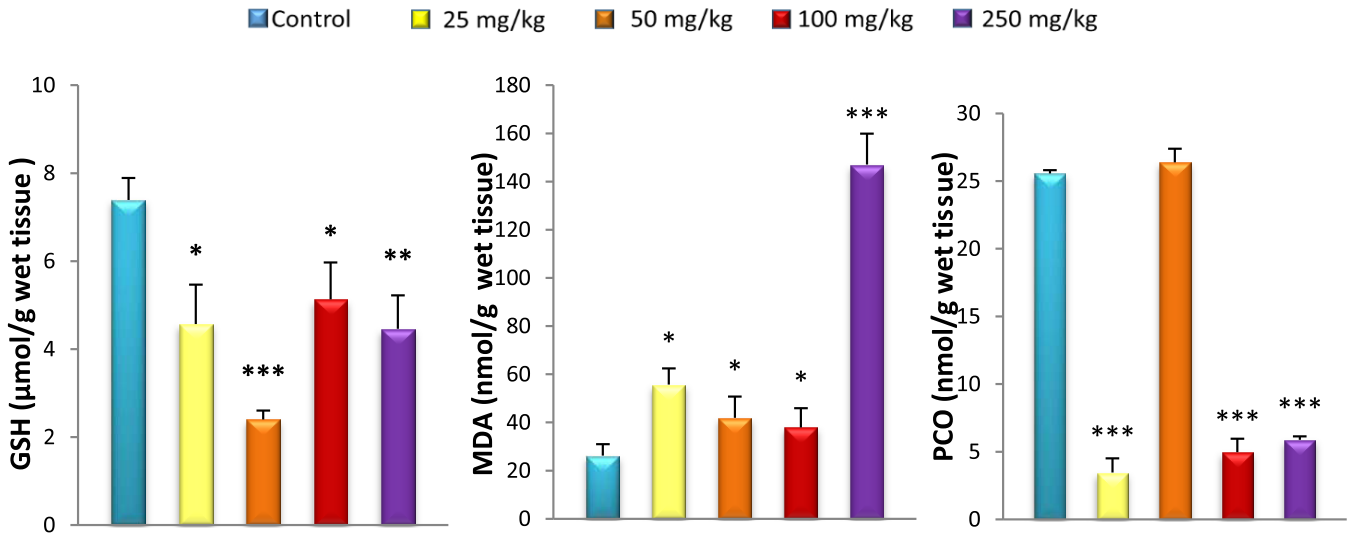

Figure 4. Effect of caudal injection of different doses of GNPs on the GSH, MDA, and PCO levels in the kidneys compared to control. Values were presented as mean ± SD. *$P < 0.05$; **$P < 0.01$; ***$P < 0.001$.

https://doi.org/10.1021/acsomega.2c00727
ACS Omega 2022, 7, 20656−20665

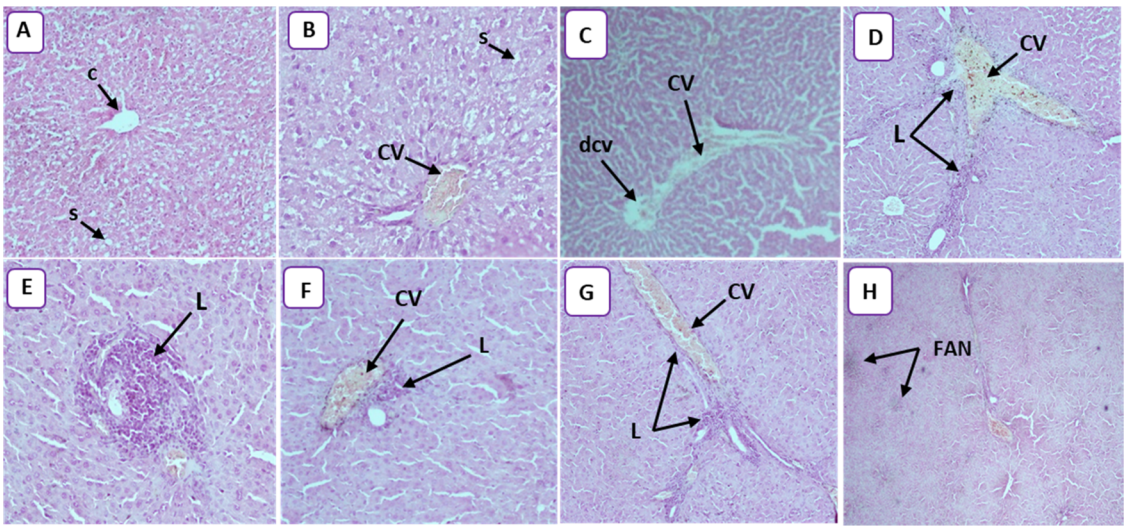

Figure 5. (A) Photomicrograph of control rats, showing the normal histological architecture of liver tissue (HEX10). The central vein (C) is surrounded by hepatic cells separated by blood sinusoids (s). (B) Photomicrograph of the rat liver treated with 25 mg/kg (HEX20) showing congestive vessel (CV) and narrowing of the sinusoidal lumen (S). (C) Photomicrograph of rat liver treated with 50 mg/kg (HEX4) showing congestive vessel (CV) and dilated central vein (DCV). (D) Photomicrograph of rat liver treated with 100 mg/kg (HEX10) showing congestive vessel (CV) and lymphocytic infiltration (L). (E) Photomicrograph of rat liver treated with 100 mg/kg (HEX20) showing lymphocytic infiltration (L) and inflammation. (F) Photomicrograph of rat liver treated with 100 mg/kg (HEX10) showing congestive vessel (CV) and lymphocytic infiltration (L) and inflammation. (G) Photomicrograph of rat liver treated with 250 mg/kg (HEX10) showing congestive vessel (CV) and lymphocytic infiltration (L). (H) Photomicrograph of rat liver treated with 250 mg/kg (HEX10) showing focal areas of necrosis (FAN).

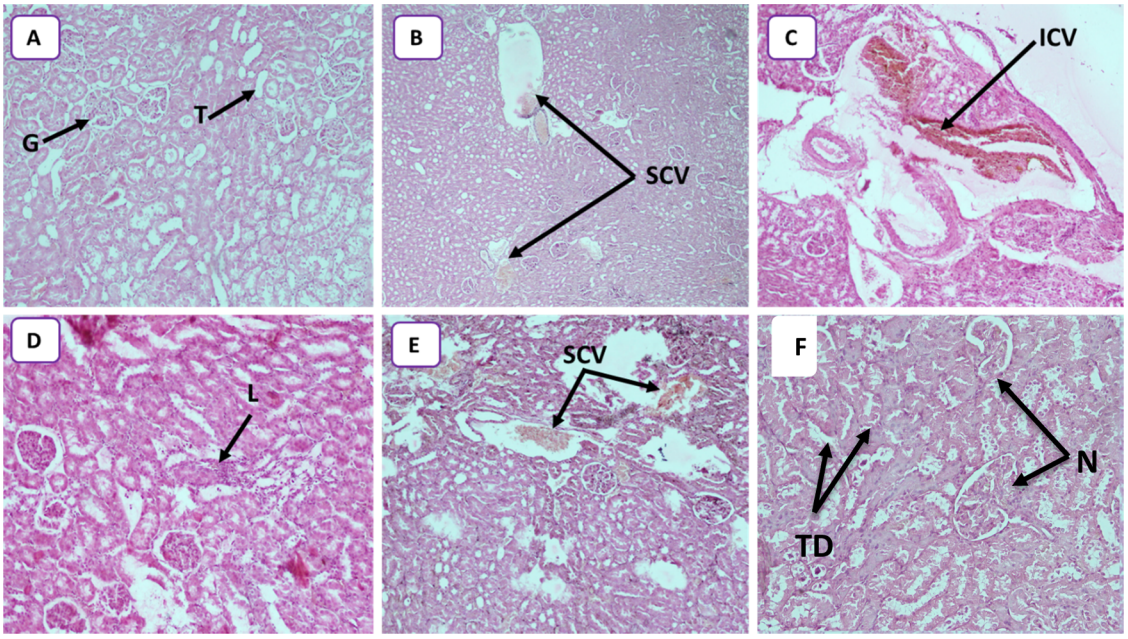

Figure 6. (A) Photomicrograph of control rats, showing normal structure kidney tissues with glomerulus (G) and tubules (T) (HEX10). (B) Photomicrograph of the rat kidneys treated with 25 mg/kg (HEX4) showing several congestive vessels (SCVs). (C) Photomicrograph of the rat kidneys treated with 50 mg/kg (HEX10) showing important congestive vessels (ICVs). (D) Photomicrograph of the rat kidneys treated with 50 mg/kg (HEX10) showing lymphocytic infiltration (L). (E) Photomicrograph of the rat kidneys treated with 100 mg/kg (HEX10) showing several congestive vessels (SCVs). (F) Photomicrograph of the rat kidneys treated with 250 mg/kg (HEX10) showing tubular degeneration (TD) and necrotic state (N).

circulating GSH, organs such as the kidneys salvage GSH.[41] In this study, the hepatic GSH level remained unchanged for all GNP-treated rats compared to controls despite oxidative stress marked by elevated MDA. Khan et al.[42] found the same results in the liver after injection of GNPs with a size of 10 nm. Our results also show the liver lesions in histopathological observation. This can be explained by the inability of the liver to increase GSH levels in response to this oxidative stress. In fact, low levels of GSH result from the inability of the liver to cope with different toxic metabolites such as electrophiles as well as lipid peroxides responsible for tissue damage.[43,44] Unable to overproduce GSH, plasma and kidneys cannot increase GSH levels from the liver. This explains our results, which show decreased GSH levels in plasma and kidneys for all

https://doi.org/10.1021/acsomega.2c00727
ACS Omega 2022, 7, 20656−20665

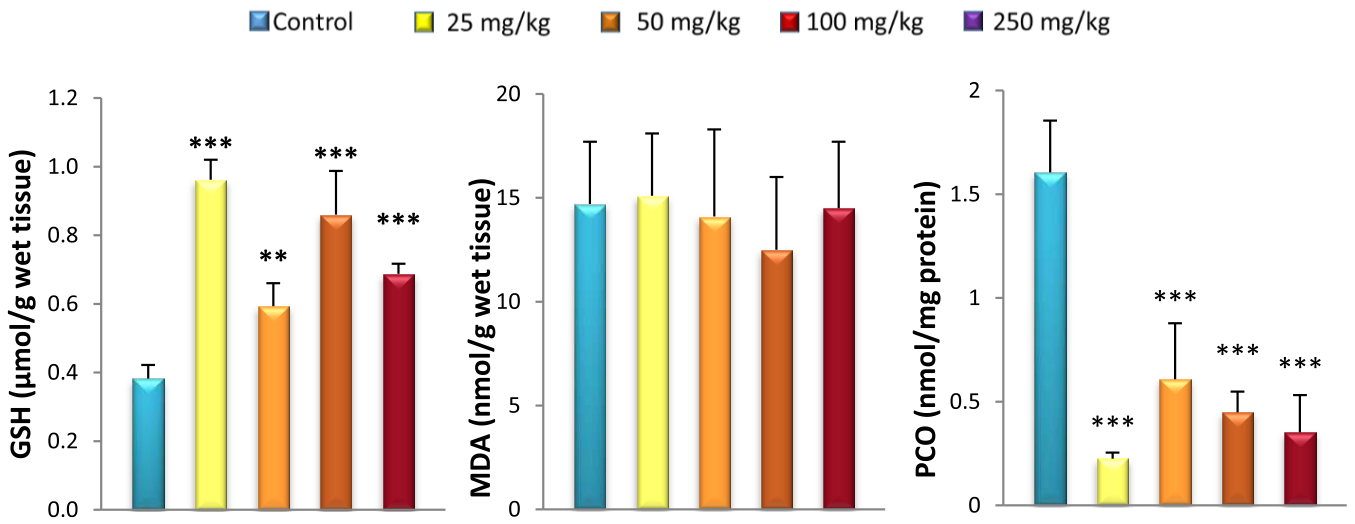

Figure 7. Effect of caudal injection of different doses of GNPs on the brain GSH, MDA, and PCO levels compared to control. Values were presented as mean ± SD. $^{**}P < 0.01$; $^{***}P < 0.001$.

GNP doses used. The depletion of GSH from cells leads to lipoxygenase (LOX) activation, ROS production from mitochondria, and calcium influx, which initiate a form of programmed cell death with features of both apoptosis and necrosis.[45,46] The lack of GSH is also reflected by the increase in MDA in the plasma, kidneys, and liver of all GNP-treated rats. The decrease in GSH levels results in the overproduction of free radicals that leads to lipid peroxidation, particularly in cell membranes,[47] which can change membrane integrity and lead to tissue damage.[48] Previous studies have reported no MDA changes in plasma, kidneys, and liver 24 h after GNP administration. Our results show that lipid peroxidation is detectable 15 days after GNP injection (Figures 2−5).[49,50]

The amounts of carbonyl protein in the liver and kidneys after treatment with 25, 100, and 250 mg/kg GNPs were low compared to those in controls, reflecting an imbalance in the redox status. It has previously been demonstrated that when the cell was exposed to oxidative stress, protein glutathionylation was induced. This protected proteins from oxidation and explained the low PCO levels.[51,52] Protein glutathionylation induced loss of protein function, which caused cellular alterations.[53]

Kidney injury was observed in the histopathological study. The degree of alteration increased with nanoparticle dose, ranging from congestion at 25 mg/kg to lymphocytic infiltration at 50 mg/kg and ending in tubular degeneration and a necrotic state at 250 mg/kg (Figure 6A−F). Abdelhalim et al.[54] observed a similar phenomenon of inflammatory cell infiltration in the renal tissue at a GNP concentration of 50 mg/kg. The infiltrating cells were mainly neutrophils and mononuclear cells. The presence of inflammatory cells in the renal tissue confirmed that the GNPs could interact with proteins and enzymes of the renal interstitial tissue. The interaction of GNPs with these biomolecules could disrupt the antioxidant defense machinery, which resulted in ROS generation that imitated an inflammatory response. A similar phenomenon of more immunological responses with smaller GNPs was observed by Yen et al.[14] and Pan et al.[11] for smaller-size NPs. Our results were in line with these earlier findings and confirmed that the smaller-size GNPs generated higher toxicity owing to the increased surface reactivity of GNPs.[55,55] Furthermore, histological alterations in renal tissue caused by these particles make it impossible to deal with the accumulated residues resulting from metabolic and structural disturbances. The decrease in the activity of the kidneys causes the GNPs to recirculate in the bloodstream. All treated rats showed several large congestive vessels, particularly rats treated with 250 mg/kg of GNPs.

The treated animals showed distinct morphological changes in the liver upon microscopic observation compared to the control group, indicating unhealthy cells. All treated rats showed congestive vessels with or without a dilated vein. Moreover, infiltration was noticed in the animals treated with 100 and 250 mg/kg GNPs (Figure 5D−G). Park et al.[56] demonstrated that silver nanoparticles released into the bloodstream accumulated toxic effects in the liver, kidneys, and heart, causing scattered cytoplasmic vacuolization, appearance of chronic inflammatory cells, and congested and dilated blood vessels. The presence of inflammatory cells in the hepatic tissue reveals the interaction of GNPs with proteins and enzymes in the interstitial tissue of the liver, resulting from the failure of the antioxidant defense machinery. The erasure of radial architecture in the liver of treated animals (250 mg/kg; Figure 5H) showed necrosis. The GNP-induced necrosis was predominantly attributed to their ability to evoke ROS production,[57] and it led to hepatocyte necrosis in treated animals. Only rats treated with 250 mg/kg GNPs showed necrosis in the current work.

The response of the brain to oxidative stress is different from those of the liver and kidneys. High levels of glutathione (GSH) were seen in the brain of all GNP-treated rats (Figure 7). This can be an adaptive mechanism in response to GNP exposure. Specific chelators and subsequent sequestration of metal complexes are of particular interest to lower the concentrations of transition metals.[56] GSH is a precursor of phytochelatins; hence, it is an essential element for metal scavenging because of the higher affinity of metal NPs towards the thiol (−SH) group.[58,59] It seems that GSH levels increase specifically in the brain compared to those in other organs (kidneys and liver). The cellular GSH concentration is maintained by a complex homeostatic mechanism wherein the steady-state concentration is under the kinetic control of

https://doi.org/10.1021/acsomega.2c00727
ACS Omega 2022, 7, 20656−20665

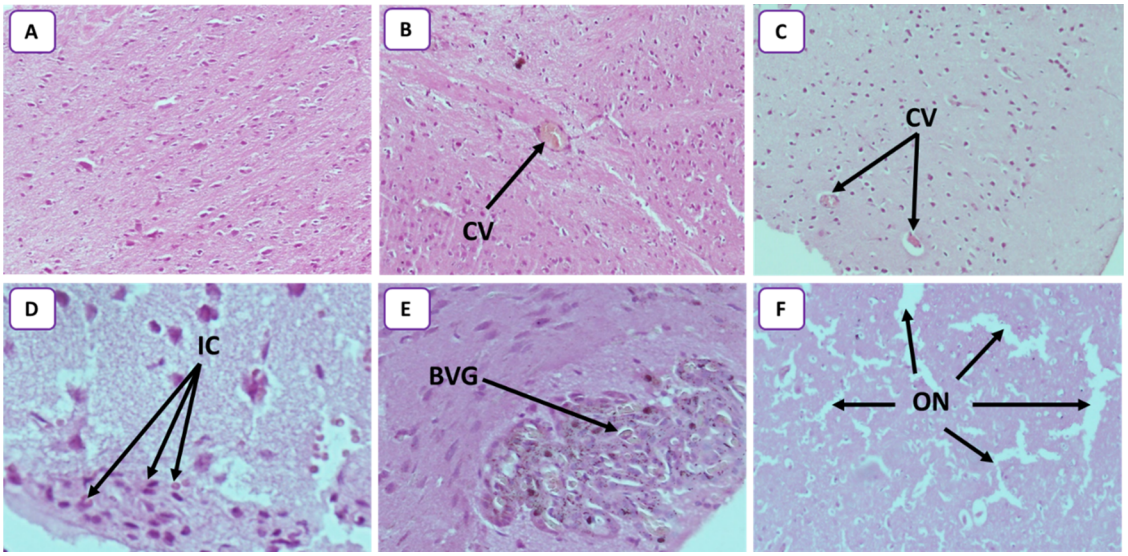

Figure 8. (A) Photomicrograph of control rats, showing normal glial cells without inflammation or congestion (HEX10). (B) Photomicrograph of the rat brain treated with 25 mg/kg (HEX10) showing a congestive vessel (CV). (C) Photomicrograph of the rat brain treated with 50 mg/kg (HEX10) showing two congestive vessels (CVs). (D) Photomicrograph of the rat brain treated with 50 mg/kg (HEX40) showing some inflammatory cells (ICs). (E) Photomicrograph of rat brain treated with 100 mg/kg (HEX40) showing blood vessel with glomeruloid aspect (BVG). (F) Photomicrograph of rat brain treated with 250 mg/kg (HEX10) showing several outbreaks of necrosis (ON) highlighted by the glial cell space.

specific enzymatic reactions.[60] The GSH concentration is also controlled by the rate of oxidation, conjugation, extrusion, uptake of thiol-containing precursors, and resynthesis.[61] It is likely that there is a regulation of GSH level in the brain by one or more of these mechanisms. Increased GSH in the brain is associated with low PCO rates. Pocernich et al.[62] demonstrated that glutathione elevation protected against hydroxyl free-radical-induced protein oxidation in rat brains. Adeyemi et al.[63] observed a decrease in brain PCO levels in the rat after oral administration of silver. The MDA rate is also reduced by the GSH's share in the brain. Indeed, GSH is a cofactor for glutathione peroxidase that catalyses the reduction of hydrogen peroxide to water and oxygen, hence limiting the formation of hydroxyl radicals. This reaction, in the presence of GSH, helps to limit lipid peroxidation, thus reducing the production of MDA.[64] The protective effect of GSH against lipid peroxidation and a decrease in PCO do not prevent the appearance of alterations in the brain. Low PCO can be a consequence of protein glutathionylation.[51,52] Protein glutathionylation induces loss of protein function, which causes cellular alterations.[53] Alterations in the brain tissue are observed by histopathology (Figure 8) and the results are summarized as follows: the congestive vessel is observed in rats treated with 25 and 50 mg/kg GNPs (Figure 8B,C) and inflammatory cells are observed in rats treated with 50 and 100 mg/kg GNPs (Figure 8D,E). Reduced glutathione, in addition to its action as a transition-metal chelator, in protection against lipid peroxidation, and in protein carboxylation, is also considered a chemical mediator of inflammation. It has been shown that the intracellular GSH status plays a critical role in regulating monocyte-to-macrophage differentiation and inflammation.[65] This explains the inflammatory state found in the brain. In fact, multiple inflammatory cells can migrate to the brain during an inflammatory response such as T and B lymphocytes, macrophages, and monocytes.[66,67]

The internalization of GNPs in the brain tissue was well elaborated on by many researchers; for example, De Jong et al.[68] studied the GNP-size-dependent tissue distribution in the brain 24 h postinjection in rats. The study reveals that GNPs with the smallest size of 10 nm accumulated in the brain tissues more than the bigger-size GNPs. On the other hand, Hillyer et al.[69] interestingly observed that the single oral administration of GNPs (from 4 to 58 nm) can pass the blood−brain barrier and accumulate in the brain tissues. The passage of GNPs in treated rat brains results in the uptake across the BBB after its permutation from the blood, leading to systemic exposure to the brain.[70] When NPs enter the circulation system, their influence on the endothelial cell membrane results in cytotoxicity and/or breaking of tight junctions of the BBB, which further opens an entry into the cerebral environment for NPs.[71] Similarly, it was found that aluminum (Al), silver (Ag), and Cu nanoparticles significantly altered the BBB in several regions of the brain and spinal cord of mice and rats.[71] It is presumed that a healthy BBB contains defense mechanisms to protect the brain from blood-borne pathogens or NP exposure.

When NPs with different surface characteristics were assessed, chargeless NPs and low concentrations of anionic NPs did not affect the BBB integrity. However, high concentrations of anionic NPs and even low concentrations of cationic NPs can disrupt the BBB.[72] Many possible mechanisms for NPs toxicity have been described earlier including injury of epithelial tissue[73] and inflammation or oxidative stress response.[34] Oxidative stress is the most important cytotoxic initiator for all the cells.[74] GNPs are also responsible for activating 8-hydroxydeoxyguanosine (8OHdG), caspase 3 and heat shock protein 70 (Hsp70), and IFN-γ. These biochemical processes result in inflammation and DNA damage that finally cause cell death. Compared with the results of Siddiqi et al.,[75] who found alterations in the brain of mice injected with 20 μg/kg of gold nanoparticles for 3 days, our results show brain damage only at the highest dose (250 mg/kg) (Table 2).

https://doi.org/10.1021/acsomega.2c00727
ACS Omega 2022, 7, 20656−20665

Table 2. Main Findings of the Studies on Histopathology Changes in Different Tissues of the Brain, Liver, and Kidneys of Wistar Rats at Different Doses of Small-Size GNPs (c. 20 nm)

organ	dose of gold nanoparticle	histological result
brain	25, 50, and 100 mg/kg	inflammatory cells and congestive vessel
	250 mg/kg	several outbreaks of necrosis highlighted by the glial cell space
liver	25 and 50 mg/kg	congestive vessel
	100 mg/kg	lymphocytic infiltration, inflammation, and congestive vessel
	250 mg/kg	congestive vessel, lymphocytic infiltration, and focal areas of necrosis
kidneys	25 mg/kg	congestive vessels
	50 mg/kg	lymphocytic infiltration and congestive vessels
	100 mg/kg	several congestive vessels
	250 mg/kg	tubular degeneration and necrotic state

4. CONCLUSIONS

The results of this study reveal the impact of gold nanoparticle doses on different tissues. The findings contribute to deepening our understanding of oxidative stress and the cellular interaction by nanoparticles. Our data show that GNPs induce an imbalance in the oxidant/antioxidant system marked by variations in GSH, MDA, and PCO levels. These variations are different for different organs where the levels of glutathione affect the levels of MDA and PCO levels. As a result of the oxidant/antioxidant imbalance, histological alterations are present after the 15th day of GNP administration. These are significant at 250 mg/kg but minimal at the lower doses of 25, 50, and 100 mg/kg, where necrosis is absent.

AUTHOR INFORMATION

Corresponding Author

Nanasaheb D. Thorat − *Nuffield Department of Women's & Reproductive Health, John Radcliffe Hospital, Medical Sciences Division, University of Oxford, Oxford OX3 9DU, U.K.; Faculty of Engineering and Sciences, MIT Art, Design and Technology University, Pune 412201 Maharashtra, India;* orcid.org/0000-0001-6343-527X; Email: thoratnd@gmail.com

Authors

Bekhti Sari Fadia − *Laboratory of Physiology, Pathophysiology and Biochemistry of Nutrition, Department of Biology, Faculty of Natural and Life Sciences, Earth and Universe, University of Tlemcen, Tlemcen 13000, Algeria*

Nassima Mokhtari-Soulimane − *Laboratory of Physiology, Pathophysiology and Biochemistry of Nutrition, Department of Biology, Faculty of Natural and Life Sciences, Earth and Universe, University of Tlemcen, Tlemcen 13000, Algeria*

Bensalah Meriem − *Laboratory of Physiology, Pathophysiology and Biochemistry of Nutrition, Department of Biology, Faculty of Natural and Life Sciences, Earth and Universe, University of Tlemcen, Tlemcen 13000, Algeria*

Nacer Wacila − *Laboratory of Physiology, Pathophysiology and Biochemistry of Nutrition, Department of Biology, Faculty of Natural and Life Sciences, Earth and Universe, University of Tlemcen, Tlemcen 13000, Algeria*

Badi Zouleykha − *Laboratory of Physiology, Pathophysiology and Biochemistry of Nutrition, Department of Biology, Faculty of Natural and Life Sciences, Earth and Universe, University of Tlemcen, Tlemcen 13000, Algeria*

Rouigueb Karima − *Laboratory of Physiology, Pathophysiology and Biochemistry of Nutrition, Department of Biology, Faculty of Natural and Life Sciences, Earth and Universe, University of Tlemcen, Tlemcen 13000, Algeria*

Tewfik Soulimane − *Modelling Simulation and Innovative Characterisation (MOSAIC), Department of Chemical Engineering, and Bernal Institute, University of Limerick, Limerick V94 T9PX, Ireland*

Syed A. M. Tofail − *Modelling Simulation and Innovative Characterisation (MOSAIC), Department of Physics, School of Natural Sciences and Bernal Institute, University of Limerick, Limerick V94 T9PX, Ireland*

Helen Townley − *Nuffield Department of Women's & Reproductive Health, John Radcliffe Hospital, Medical Sciences Division, University of Oxford, Oxford OX3 9DU, U.K.*

Complete contact information is available at: https://pubs.acs.org/10.1021/acsomega.2c00727

Notes

The authors declare no competing financial interest.

ACKNOWLEDGMENTS

N.D.T. and H.T. acknowledge that the project leading to this research has received funding from the European Union's Horizon 2020 Research and Innovation Programme under the Marie Sklodowska-Curie Grant Agreement No. 840964 "SUPERBRAIN". The authors are thankful to Dr. Hadjmerabet Djahida for the support during manuscript preparation.

REFERENCES

(1) Barnes, C. A.; Elsaesser, A.; Arkusz, J.; Smok, A.; Palus, J.; Leśniak, A.; Salvati, A.; Hanrahan, J. P.; Jong, W. H.; Dziubałtowska, E.; Stepnik, M.; Rydzyński, K.; McKerr, G.; Lynch, I.; Dawson, K. A.; Howard, C. V. Reproducible comet assay of amorphous silica nanoparticles detects no genotoxicity. *Nano Lett.* **2008**, *8*, 3069−3074.

(2) El-Sayed, I. H.; Huang, X.; El-Sayed, M. A. Surface Plasmon Resonance Scattering and Absorption of Anti-EGFR Antibody Conjugated Gold Nanoparticles in Cancer Diagnostics: Applications in Oral Cancer. *Nano Lett.* **2005**, *5*, 829−834.

(3) Ghosh, P.; Han, G.; De, M.; Kim, C. K.; Rotello, V. M. Gold Nanoparticles in Delivery Applications. *Adv. Drug Delivery Rev.* **2008**, *60*, 1307−1315.

(4) Chithrani, D. B.; Jelveh, S.; Jalali, F.; Van Prooijen, M.; Allen, C.; Bristow, R. G.; Hill, R. P.; Jaffray, D. A. Gold Nanoparticles as Radiation Sensitizers in Cancer Therapy. *Radiat. Res.* **2010**, *173*, 719−728.

(5) Hainfeld, J. F.; Dilmanian, F. A.; Slatkin, D. N.; Smilowitz, H. M. Radiotherapy Enhancement with Gold Nanoparticles. *J. Pharm. Pharmacol.* **2010**, *60*, 977−985.

(6) (a) Huang, X.; Jain, P. K.; El-Sayed, I. H.; El-Sayed, M. A. Plasmonic Photothermal Therapy (PPTT) Using Gold Nanoparticles. *Lasers Med. Sci.* **2008**, *23*, 217−228. (b) Thorat, N. D.; Dworniczek, E.; Brennan, G.; Chodaczek, G.; Mouras, R.; Gascón Pérez, V.; Silien, C.; Tofail Syed, A. M.; Bauer, J. Photo-responsive functional gold nanocapsules for inactivation of community-acquired, highly virulent, multidrug-resistant MRSA. *J. Mater. Chem. B* **2021**, *9*, 846−856. (c) Brennan, G.; Thorat, N. D.; Pescio, M.; Bergamino, S.; Bauer, J.; Liu, N.; Tofail Syed, A. M.; Silien, C. Spectral drifts in surface textured Fe3O4-Au, core−shell nanoparticles enhance spectra-selective photo-

thermal heating and scatter imaging. *Nanoscale* **2020**, *12*, 12632−12638.
(7) Ma, N.; Wu, F. G.; Zhang, X.; Jiang, Y. W.; Jia, H. R.; Wang, H. Y.; Chen, Z.; et al. Shape-dependent radiosensitization effect of gold nanostructures in cancer radiotherapy: comparison of gold nanoparticles, nanospikes, and nanorods. *ACS Appl. Mater. Interfaces* **2017**, *9*, 13037−13048.
(8) Yu, L. E.; Yung, L. Y. L.; Ong, C. N.; Tan, Y. L.; Balasubramaniam, K. S.; Hartono, D.; Shui, G.; Wenk, M. R.; Ong, W. Y. Translocation and Effects of Gold Nanoparticles after Inhalation Exposure in Rats. *Nanotoxicology* **2007**, *1*, 235−242.
(9) Lanone, S.; Boczkowski, J. Biomedical Applications and Potential Health Risks of Nanomaterials: Molecular Mechanisms. *Curr. Mol. Med.* **2006**, *6*, 651−663.
(10) BarathManiKanth, S.; Kalishwaralal, K.; Sriram, M.; Pandian, S. B. R. K.; Youn, H. S.; Eom, S. H.; Gurunathan, S. Anti-Oxidant Effect of Gold Nanoparticles Restrains Hyperglycemic Conditions in Diabetic Mice. *J. Nanobiotechnol.* **2010**, *8*, No. 16.
(11) Pan, Y.; Neuss, S.; Leifert, A.; Fischler, M.; Wen, F.; Simon, U.; Schmid, G.; Brandau, W.; Jahnen-Dechent, W. Size-Dependent Cytotoxicity of Gold Nanoparticles. *Small* **2007**, *3*, 1941−1949.
(12) Takahashi, H.; Niidome, Y.; Niidome, T.; Kaneko, K.; Kawasaki, H.; Yamada, S. Modification of Gold Nanorods Using Phosphatidylcholine to Reduce Cytotoxicity. *Langmuir* **2006**, *22*, 2−5.
(13) De Jong, W. H.; Borm, P. J. A. Drug Delivery and Nanoparticles: Applications and Hazards. *Int. J. Nanomed.* **2008**, 133−149.
(14) Yen, H. J.; Hsu, S. H.; Tsai, C. L. Cytotoxicity and Immunological Response of Gold and Silver Nanoparticles of Different Sizes. *Small* **2009**, *5*, 1553−1561.
(15) Abdelhalim, M.; Jarrar, B. M. Gold Nanoparticles Administration Induced Prominent Inflammatory, Central Vein Intima Disruption, Fatty Change and Kupffer Cells Hyperplasia. *Lipids Health Dis.* **2011**, *10*, No. 133.
(16) Lasagna-Reeves, C.; Gonzalez-Romero, D.; Barria, M. A.; Olmedo, I.; Clos, A.; Sadagopa Ramanujam, V. M.; Urayama, A.; Vergara, L.; Kogan, M. J.; Soto, C. Bioaccumulation and Toxicity of Gold Nanoparticles after Repeated Administration in Mice. *Biochem. Biophys. Res. Commun.* **2010**, *393*, 649−655.
(17) Han, S. G.; Lee, J. S.; Ahn, K.; Kim, Y. S.; Kim, J. K.; Lee, J. H.; Shin, J. H.; Jeon, K. S.; Cho, W. S.; Song, N. W.; Gulumian, M.; Shin, B. S.; Yu, I. J. Size-Dependent Clearance of Gold Nanoparticles from Lungs of Sprague−Dawley Rats after Short-Term Inhalation Exposure. *Arch. Toxicol.* **2015**, *89*, 1083−1094.
(18) Cho, W. S.; Cho, M.; Jeong, J.; Choi, M.; Cho, H. Y.; Han, B. S.; Kim, S. H.; Kim, H. O.; Lim, Y. T.; Chung, B. H.; Jeong, J. Acute Toxicity and Pharmacokinetics of 13 Nm-Sized PEG-Coated Gold Nanoparticles. *Toxicol. Appl. Pharmacol.* **2009**, *236*, 16−24.
(19) Ibrahim, K. E.; Al-Mutary, M. G.; Bakhiet, A. O.; Khan, H. A. Histopathology of the Liver, Kidney, and Spleen of Mice Exposed to Gold Nanoparticles. *Molecules* **2018**, *23*, No. 1848.
(20) Du, Z. X.; Zhang, H. Y.; Meng, X.; Guan, Y.; Wang, H. Q. Role of oxidative stress and intracellular glutathione in the sensitivity to apoptosis induced by proteasome inhibitor in thyroid cancer cells. *BMC Cancer* **2009**, *9*, 56.
(21) Tedesco, S.; Doyle, H.; Blasco, J.; Redmond, G.; Sheehan, D. Oxidative stress and toxicity of gold nanoparticles in Mytilus edulis. *Aquat. Toxicol.* **2010**, *100*, 178−186.
(22) Babaei Afrapoli, Z.; Majidi, R. F.; Negahdari, B.; Tavoosidana, G. 'Inversed Turkevich' Method for Tuning the Size of Gold Nanoparticles: Evaluation the Effect of Concentration and Temperature. *Nanomed. Res. J.* **2018**, *3*, 190−196.
(23) Matamoros-Ambrocio, M.; Ruiz-Peralta, M.; Chigo-Anota, E.; García-Serrano, J.; Pérez-Centeno, A.; Sánchez-Cantú, M.; Rubio-Rosas, E.; Escobedo-Morales, A. A Comparative Study of Gold Impregnation Methods for Obtaining Metal/Semiconductor Nanophotocatalysts: Direct Turkevich, Inverse Turkevich, and Progressive Heating Methods. *Catalysts* **2018**, *8*, 161.
(24) Fischer, A. H.; Jacobson, K. A.; Rose, J.; Zeller, R. Cutting Sections of Paraffin-Embedded Tissues. *Cold Spring Harbor Protoc.* **2008**, *2008*, No. pdb-rot4987.
(25) Ellman, G. L. Tissue sulfhydryl groups. *Arch. Biochem. Biophys.* **1959**, *82*, 70−77.
(26) Draper, H. H.; Hadley, M. Malondialdehyde determination as index of lipid Peroxidation. *Methods Enzymol.* **1990**, *186*, 421−431.
(27) Levine, R. L.; Garland, D.; Oliver, C. N.; Amici, A.; Climent, I.; Lenz, A. G.; Stadtman, E. R.; et al. Determination of carbonyl content in oxidatively modified proteins. *Methods Enzymol.* **1990**, *186*, 464−478.
(28) Underwood, J. C. E. Histochemistry. Theoretical and Applied. *J. Pathol.* **1985**, *147*, 234−234.
(29) Ebrahimpour, Z.; Mansour, N. Annealing. Effects on Electrical Behavior of Gold Nanoparticle Film: Conversion of Ohmic to Non-Ohmic Conductivity. *Appl. Surf. Sci.* **2017**, *394*, 240−247.
(30) Shi, Y.; Evans, J. E.; Rock, K. L. Molecular identification of a danger signal that alerts the immune system to dying cells. *Nature* **2003**, *425*, 516−521.
(31) Kanellis, J.; Watanabe, S.; Li, J. H.; Kang, D. H.; Li, P.; Nakagawa, T.; Johnson, R. J.; et al. Uric acid stimulates monocyte chemoattractant protein-1 production in vascular smooth muscle cells via mitogen-activated protein kinase and cyclooxygenase-2. *Hypertension* **2003**, *41*, 1287−1293.
(32) Mazzali, M.; Hughes, J.; Kim, Y. G.; Jefferson, J. A.; Kang, D. H.; Gordon, K. L.; Johnson, R. J.; et al. Elevated uric acid increases blood pressure in the rat by a novel crystal-independent mechanism. *Hypertension* **2001**, *38*, 1101−1106.
(33) Li, Y. F.; Chen, C. Fate and Toxicity of Metallic and Metal-Containing Nanoparticles for Biomedical Applications. *Small* **2011**, *7*, 2965−2980.
(34) Nel, A.; Xia, T.; Mädler, L.; Li, N. Toxic Potential of Materials at the Nanolevel. *Science* **2006**, *311*, 622−627.
(35) Tarnuzzer, R. W.; Colon, J.; Patil, S.; Seal, S. Vacancy Engineered Ceria Nanostructures for Protection from Radiation-Induced Cellular Damage. *Nano Lett.* **2005**, *5*, 2573−2577.
(36) Tian, F.; Clift, M. J. D.; Casey, A.; del Pino, P.; Pelaz, B.; Conde, J.; Byrne, H. J.; Rothen- Rutishauser, B.; Estrada, G.; de la Fuente, J. M.; Stoeger, T. Investigating the role of shape on the biological impact of gold nanoparticles in vitro. *Nanomedicine* **2015**, *10*, 2643−2657.
(37) Lopez-Chaves, C.; Soto-Alvaredo, J.; Montes-Bayon, M.; Bettmer, J.; Llopis, J.; Sanchez-Gonzalez, C. Gold nanoparticles: distribution, bioaccumulation and toxicity. *In vitro* and *in vivo* studies. *Nanomedicine* **2018**, *14*, 1−12.
(38) Mozdzan, M.; Szemraj, J.; Rysz, J.; Nowak, D. Antioxidant properties of carnosine re-evaluated with oxidizing systems involving iron and copper ions. *Basic Clin. Pharmacol. Toxicol.* **2005**, *96*, 352−360.
(39) Michelet, F.; Gueguen, R.; Leroy, P.; Wellman, M.; Nicolas, A.; Sies, G. Blood and plasma glutathione measured in healthy subjects by HPLC: relation to sex, aging; biological variances and live habits. *Clin. Chem.* **1995**, *41*, 1509−1517.
(40) Bruno, L. Le glutathion est vital; science, nutrition, prévention et santé. *Cancer Res.* **2006**, *66*, 613−621.
(41) Deneke, S. M.; Fanburg, B. L. Regulation of cellular glutathione. *Am. J. Physiol.: Lung Cell. Mol. Physiol.* **1989**, *257*, L163−L173.
(42) Khan, H. A.; Abdelhalim, M. A. K.; Al-Ayed, M. S.; Alhomida, A. S. Effect of gold nanoparticles on glutathione and malondialdehyde levels in liver, lung and heart of rats. *Saudi J. Biol. Sci.* **2012**, *19*, 461−464.
(43) Duke, R. C.; Ojcius, D. M.; Young, J. D. E. Cell suicide in health and disease. *Sci. Am.* **1996**, *275*, 80−87.
(44) Saka, S.; Bairi, A.; Guellati, M. Relations immuno-corticotropes dans un environnement nociceptif chez la rate wistar. *J. Soc. Biol.* **2003**, *197*, 67−71.

https://doi.org/10.1021/acsomega.2c00727
ACS Omega 2022, 7, 20656−20665

(45) Shirlee Tan, B. S. P.; Schubert, D.; Maher, P. Oxytosis: a novel form of programmed cell death. *Curr. Top. Med. Chem.* **2001**, *1*, 497−506.
(46) Maher, P.; van Leyen, K.; Dey, P. N.; Honrath, B.; Dolga, A.; Methner, A. The role of Ca2+ in cell death caused by oxidative glutamate toxicity and ferroptosis. *Cell. Calcium* **2018**, *70*, 47−55.
(47) Şahin, E.; Gümüşlü, S. Immobilization stress in rat tissues: alterations in protein oxidation, lipid peroxidation and antioxidant defense system. *Comp. Biochem. Physiol., Part C: Toxicol. Pharmacol.* **2007**, *144*, 342−347.
(48) Bandegi, A. R.; Rashidy-Pour, A.; Vafaei, A. A.; Ghadrdoost, B. Protective effects of Crocus sativus L. extract and crocin against chronic-stress induced oxidative damage of brain, liver and kidneys in rats. *Adv. Pharm. Bull.* **2014**, *4*, 493.
(49) Ferreira, G. K.; Cardoso, E.; Vuolo, F. S.; Michels, M.; Zanoni, E. T.; Carvalho-Silva, M.; da Silva Paula, M. M.; et al. Gold nanoparticles alter parameters of oxidative stress and energy metabolism in organs of adult rats. *Biochem. Cell Biol.* **2015**, *93*, 548−557.
(50) Hassan, A. A.; Abdoon, A. S. S.; Elsheikh, S. M.; Khairy, M. H.; Gamaleldin, A. A.; Elnabtity, S. M. Effect of acute gold nanorods on reproductive function in male albino rats: histological, morphometric, hormonal, and redox balance parameters. *Environ. Sci. Pollut. Res.* **2019**, *26*, 15816−15827.
(51) Chouchani, E. T.; James, A. M.; Fearnley, I. M.; Lilley, K. S.; Murphy, M. P. Proteomic approaches to the characterization of protein thiol modification. *Curr. Opin. Chem. Biol.* **2011**, *15*, 120−128.
(52) Burgoyne, J. R.; Eaton, P. Contemporary techniques for detecting and identifying proteins susceptible to reversible thiol oxidation. *Biochem. Soc. Trans.* **2011**, *39*, 1260−1267.
(53) Dalle-Donne, I.; Rossi, R.; Giustarini, D.; Colombo, R.; Milzani, A. S-glutathionylation in protein redox regulation. *Free Radical Biol. Med.* **2007**, *43*, 883−898.
(54) Abdelhalim, M. A. K.; Jarrar, B. M. The Appearance of Renal Cells Cytoplasmic Degeneration and Nuclear Destruction Might Be an Indication of GNPs Toxicity. *Lipids Health Dis.* **2011**, *10*, 147.
(55) Chen, X.; Schluesener, H. J. Nanosilver: A Nanoproduct in Medical Application. *Toxicol. Lett.* **2008**, *176*, 1−12.
(56) Park, E. J.; Bae, E.; Yi, J.; Kim, Y.; Choi, K.; Lee, S. H.; Yoon, J.; Lee, B. C.; Park, K. Repeated-Dose Toxicity and Inflammatory Responses in Mice by Oral Administration of Silver Nanoparticles. *Environ. Toxicol. Pharmacol.* **2010**, *30*, 162−168.
(57) Fan, J. H.; Li, W. T.; Hung, W. I.; Chen, C. P.; Yeh, J. M. Cytotoxicity and Differentiation Effects of Gold Nanoparticles to Human Bone Marrow Mesenchymal Stem Cells. *Biomed. Eng. - Appl. Basis Commun.* **2011**, *23*, 141−152.
(58) Jozefczak, M.; Remans, T.; Vangronsveld, J.; Cuypers, A. Glutathione is a key player in metal-induced oxidative stress defenses. *Int. J. Mol. Sci.* **2012**, *13*, 3145−3175.
(59) Maiorino, F. M.; Maiorino, R.; Brigelius-Flohe, R.; et al. Diversity of glutathione peroxidases. *Methods Enzymol.* **1995**, *252*, 38−53.
(60) Forman, H. *Biosynthesis of Glutathione and Its Regulation*; CRC Press: Boca Raton, FL, 2018.
(61) Ursini, F.; Maiorino, M. Lipid peroxidation and ferroptosis: The role of GSH and GPx4. *Free Radical Biol. Med.* **2020**, *152*, 175−185.
(62) Pocernich, C. B.; La Fontaine, M.; Butterfield, D. A. In-vivo glutathione elevation protects against hydroxyl free radical-induced protein oxidation in rat brain. *Neurochem. Int.* **2000**, *36*, 185−191.
(63) Adeyemi, O. S.; Shittu, E. O.; Akpor, O. B.; Rotimi, D.; Batiha, G. E. S. Silver nanoparticles restrict microbial growth by promoting oxidative stress and DNA damage. *EXCLI J.* **2020**, *19*, 492.
(64) Hsu, C. H.; Chi, B. C.; Liu, M. Y.; Li, J. H.; Chen, C. J.; Chen, R. Y. Phosphine-induced oxidative damage in rats: role of glutathione. *Toxicology* **2002**, *179*, 1−8.
(65) Vasamsetti, S. B.; Karnewar, S.; Gopoju, R.; Gollavilli, P. N.; Narra, S. R.; Kumar, J. M.; Kotamraju, S. Resveratrol attenuates monocyte-to-macrophage differentiation and associated inflammation via modulation of intracellular GSH homeostasis: Relevance in atherosclerosis. *Free Radical Biol. Med.* **2016**, *96*, 392−405.
(66) Lau, P.; Joly, E. Immunological Characteristics of the Central Nervous System. *Med. Sci.* **2001**, 395−401.
(67) Ismail, M. R.; Ordi, J.; Menendez, C.; Ventura, P. J.; Aponte, J. J.; Kahigwa, E.; Hirt, R.; Cardesa, A.; Alonso, P. L. Placental Pathology in Malaria: A Histological, Immunohistochemical, and Quantitative Study. *Hum. Pathol.* **2000**, *31*, 85−93.
(68) De Jong, W. H.; Hagens, W. I.; Krystek, P.; Burger, M. C.; Sips, A. J. A. M.; Geertsma, R. E. Particle Size-Dependent Organ Distribution of Gold Nanoparticles after Intravenous Administration. *Biomaterials* **2008**, *29*, 1912−1919.
(69) Hillyer, J. F.; Albrecht, R. M. Gastrointestinal Persorption and Tissue Distribution of Differently Sized Colloidal Gold Nanoparticles. *J. Pharm. Sci.* **2001**, *90*, 1927−1936.
(70) Oberdörster, G.; Oberdörster, E.; Oberdörster, J. Nanotoxicology: An Emerging Discipline Evolving from Studies of Ultrafine Particles. *Environ. Health Perspect.* **2005**, *113*, 823−839.
(71) Sharma, H. S.; Ali, S. F.; Hussain, S. M.; Schlager, J. J.; Sharma, A. Influence of Engineered Nanoparticles from Metals on the Blood-Brain Barrier Permeability, Cerebral Blood Flow, Brain Edema and Neurotoxicity. An Experimental Study in the Rat and Mice Using Biochemical and Morphological Approaches. *J. Nanosci. Nanotechnol.* **2009**, *9*, 5055−5072.
(72) Tiwari, S.; Amiji, M. A Review of Nanocarrier-Based CNS Delivery Systems. *Curr. Drug Delivery* **2006**, *3*, 219−232.
(73) Pagan, I.; Costa, D. L.; McGee, J. K.; Richards, J. H.; Dye, J. A.; Dykstra, M. J. Metals Mimic Airway Epithelial Injury Induced by in Vitro Exposure to Utah Valley Ambient Particulate Matter Extracts. *J. Toxicol. Environ. Health, Part A* **2003**, *66*, 1087−1112.
(74) Campbell, A.; Oldham, M.; Becaria, A.; Bondy, S. C.; Meacher, D.; Sioutas, C.; Misra, C.; Mendez, L. B.; Kleinman, M. Particulate Matter in Polluted Air May Increase Biomarkers of Inflammation in Mouse Brain. *Neurotoxicology* **2005**, *26*, 133−140.
(75) Siddiqi, N. J.; Abdelhalim, M. A. K.; El-Ansary, A. K.; Alhomida, A. S.; Ong, W. Y. Identification of Potential Biomarkers of Gold Nanoparticle Toxicity in Rat Brains. *J. Neuroinflammation* **2012**, *9*, No. 123.

https://doi.org/10.1021/acsomega.2c00727
ACS Omega 2022, 7, 20656−20665